Risk of fracture in massive wooden cultural heritage objects due to dynamic environmental variations

Magdalena Soboń*[1], Łukasz Bratasz[1]

[1] Jerzy Haber Institute of Catalysis and Surface Chemistry, Polish Academy of Sciences, 30-239 Kraków, Poland

*corresponding author, magdalena.sobon@ikifp.edu.pl

This preprint has not undergone peer review any post-submission improvements or corrections. The Version of Record of this article is published in European Journal of Wood and Wood Products, and is available online at https://doi.org/10.1007/s00107-022-01841-3.

Abstract

Most of the environmental specifications to preserve valuable collections assume hygrothermal equilibrium of the object with the surrounding environment. Though the assumption is valid for most of museum interiors, it does not reflect climate conditions in historic houses and churches whose specificity lies in dynamic temperature and relative humidity (RH) variations, particularly intense in cases of operating heating systems. The present paper analyses risk of fracture in massive wooden cultural heritage objects, particularly endangered by gradients of moisture forming in their volume due to dynamic environmental variations. A two-dimensional model of a massive object made of pine wood was subjected to two types of RH variations: step and sinusoidal. The critical amplitude and duration of variations inducing crack propagation were determined for both variation types. The modelling showed that the risk of fracture was significantly higher for a sinusoidal variation than for a sudden RH drop. Therefore, sinusoidal variations should be considered the worst case condition when analysing risk of fracture in wooden objects.

Keywords: crack propagation, wood, preservation of cultural heritage, relative humidity, indoor environment

Statements and Declarations

The authors declare that they have no known competing financial interests or personal relationships that could have appeared to influence the work reported in this paper.

Acknowledgements

The authors are grateful for granting access to the computing infrastructure built in the projects POIG.02.03.00-00-028/08 "PLATON - Science Services Platform" and POIG.02.03.00-00-110/13 "Deploying high-availability, critical services in Metropolitan Area Networks (MAN-HA)"

Funding

This work received funding from the Research Council of Norway in the framework of “SyMBoL–Sustainable Management of Heritage Building in a Long-term Perspective” Project [project no. 274749] as well as from the Polish National Agency for Academic Exchange [Grant PPN/PPO/2018/1/00004/U/00001] and the statutory research fund of the Jerzy Haber Institute of Catalysis and Surface Chemistry, Polish Academy of Sciences.

Credit authorship contribution statement

LB: Conceptualization of the model, development of methodology, analysis and interpretation of the results, preparing manuscript. MS: Development and validation of the model, performing calculations, data analysis and interpretation, preparing manuscript

Introduction

For centuries wood served not only as a building material, but was commonly used by craftsmen and artisans. Wooden sculptures and objects of applied art constitute a great proportion of European cultural heritage and they are frequently found in museum collections and historic, especially religious, buildings. Climate fluctuations in the environment of wooden sculptures and other massive elements contribute to their deterioration as wood responds to these variations by gaining and losing moisture. Wood exposed to certain relative humidity (RH) and temperature conditions eventually attains a constant 'equilibrium' level of the moisture content. In a consequence of the moisture sorption, wood swells or shrinks and the dimensional response varies over its three principal anatomical axes – longitudinal (L), radial (R) and tangential (T). The tangential direction is the most responsive, whereas, in the radial direction, the moisture-related dimensional change is approximately two times smaller. In the longitudinal direction, the dimensional response is negligible.

Long-existing awareness of the correlation between climate stability and the preservation condition of wooden heritage objects was a motivation for adopting general environmental specifications for museums as decorated wood is the key representative of objects composed of humidity-sensitive materials most vulnerable to RH and temperature fluctuations. Grounds for evidence-based environmental specifications were laid in 1990s when the key mechanical parameters - stiffness, moisture expansion coefficient, strength, strain at break and yield point were quantified for a broad range of materials relevant for cultural heritage (Mecklenburg and Tumosa 1991b, Mecklenburg et al. 1998, Mecklenburg 2007), However, most of the predictive models (Mecklenburg et al. 1998; Rachwał et al. 2012) assume equilibrium of object with the surrounding environment, which is valid for slow RH variations producing little gradient of moisture content in bulk wood. In consequence, most environmental specifications to ensure the preservation of valuable collections do not take into account the environmental specificity of churches and historic houses. It is also the case of the most recent and globally influential recommendations for museums, galleries, libraries and archives by the American Society of Heating, Refrigeration and Air-conditioning Engineers ASHRAE (2019). This significant gap of knowledge in understanding how the described variations endanger massive wooden objects is addressed by the present study.

Moisture related dimensional response of massive wooden objects can be internally restrained due to two phenomena. Firstly, in the objects of a cylindrical symmetry, anisotropy of moisture related expansion coefficients leads to the suppression of tangential shrinkage or swelling due to the insufficient radial response. Secondly, as moisture diffusion in wood is not instantaneous, moisture gradients are generated in the object. For dynamic RH changes, moisture content (MC) differs in the outer and internal parts of an object, which results in their different dimensional response. Gradients of moisture content are particularly pronounced in massive objects owing to their long response times.

Dynamic RH variations are typical of historic buildings or museums with less strict climate control and can be usually associated with human activity. Churches are particularly important category of historic buildings as they usually contain valuable wooden furnishings and decorative objects. Many of them were not heated in the past but current demands of thermal comfort in churches during services or cultural events enhances the tendency to install heating systems. Similarly, concerts, social events and conferences organised in various categories of historic buildings require high level of thermal comfort. Due to economic reasons, the interior is heated rapidly for a short period. Therefore, there is a need to develop evidence-based environmental guidelines on how to manage climate during such events to minimise risk to vulnerable objects.

Moisture gradients and resulting stresses can lead to fracture of the material. Stress field in lime wood (*Tilia sp.)* cylinder was numerically modelled by Jakieła et al. (2008) using classical mechanics. By comparison of lime wood strength, determined experimentally for various RH levels, with the calculated stress, the authors calculated critical RH variations that would initiate damage of wooden cylinders simulating sculptures. However, the results do not allow to estimate the magnitude of the damage the visual impact of which is correlated with the depth and related

width of the developed crack. Another limitation of the approach proposed is that it assumed the object to be crack-free in its initial state, whereas historic wooden objects usually have accumulated numerous cracks in their history. In consequence, the approach proposed is insufficient for informing pragmatic preventive conservation where the risk of further mechanical damage to already cracked objects, as this presented in Fig. 1, is the main concern.

Fig.1 Cracked sculpture *Virgin and Child*, Nikolaus Elscheidt (possibly), c. 1859, Rijksmuseum

Since the pioneering works of Griffith (1921) and Irwin (1957), the classic elastic approach is typically used to estimate the amount of energy available for crack propagation – the energy release rate (G). Rapid crack growth occurs when G exceeds the material's property termed fracture toughness.

Porter (1964) was the first to use fracture mechanics approach to study crack development in wood. The applicability of a fracture mechanics concept to wood was later verified, amended and confirmed by Triboulot et al. (1984). As an orthotropic material, wood is characterized by six systems of crack propagation that may differ in the fracture toughness value. Schniewind and Centeno (1973) performed the first complete study of all six systems in Douglas fir. Wood's fracture toughness depends on many other factors as wood species and MC. In a review paper, Stanzl-

Tschegg et al. (1995) analysed the existing experimental data and methods, and showed a significant influence of geometrical factors of a specimen and crack orientation on the values of fracture toughness determined experimentally. The authors proposed also an optimal method for wood characterisation. Luimes et al. (2018a) analysed fracture toughness of old wood using oak samples dated back to 14th and 17^{h} centuries and compared the results to the parameter of new wood. It was demonstrated that fracture toughness of old and new wood is similar but the character of crack propagation and other mechanical properties are different.

The *J*-integral proposed by Rice in 1968 is one of the most frequently applied methods to calculate *G* in elastic materials. Since then, several authors have contributed to further development of the *J*-integral theory. Yeh and Schniewind (1992) were the first to calculate the *J*-integral in wood. Dag (2006) and Hein and Kuna (2017) proposed methods of *J*-integral calculation for Functionally Graded Materials subjected to thermal stresses generating temperature gradients in materials with continuous spatial variation of material properties. The same approach can be applied to wood with orthotropic mechanical properties, depending on MC.

In the last years, several numerical studies on climate-induced wood cracking were published (Phan 2016, Hamdi et al. 2017, Hamdi and Moutou Pitti 2018) with the most recent by Luimes and Suiker (2021) who performed numerical modelling of climate induced fracture and deformation in museum objects based on the analysis of local tensile stress field.

To the authors' knowledge, except for research performed by Jakieła et al. (2008), there is no extensive analysis of impact of dynamic RH variations on historic massive wooden objects. In the present paper, a model of massive wooden object with existing damage areas is analysed to provide information about risk of damage for cultural heritage objects due to dynamic environmental variations and to inform the preservation strategy developed by conservation professionals.

Materials and methods

Model

A model of a wooden sculpture used for calculations was created in the COMSOL Multiphysics software. A wooden sculpture was represented by an object of the cylindrical symmetry with the *z*-axis coinciding with the central axis of the tree trunk. Due to significantly higher stiffness in the L direction, the model was reduced to a 2D disc and plane strain conditions were applied according to results shown by Luimes et al. (2018b). In the two-dimensional space, the chosen polar coordinate system is synonymous with R and T directions in wood. The geometry was further limited to only half of the disc by applying symmetric conditions in terms of mechanical constraints and moisture flux as it reduced time and computational cost of calculations. The disc's diameter of 130 mm was adopted similarly to the model used by Jakieła et al. (2008). The model is presented in Fig. 2.

Crack of discrete depth ranging between 70 µm and 60 mm was introduced into the geometry and special boundary condition – Contact Pair – was applied to prevent against unphysical overlap of the crack walls. The depth of the smallest crack that could grow under given conditions was estimated using Griffith's equation for a critical flaw size *a* in mode I:

$$K_{Ic} = \sigma\sqrt{\pi a} \tag{1}$$

where K_{Ic} denotes wood's fracture toughness related to G_{Ic} (here under plane strain conditions):

$$G_{Ic} = {K_{Ic}}^2 \cdot \frac{1-\nu^2}{E} \tag{2}$$

and σ is the maximum expected stress ($\sigma = E \times \varepsilon = E \times \alpha \times \Delta RH = 725MPa \times 0.04 \times 1 = 29MPa$). E is the elasticity modulus, α is the hygric expansion coefficient and ν is the Poisson's ratio.

Crack tip is oriented in the direction normal to the T direction and it can advance towards the centre along the radius of the disc. The simplest case of moisture diffusion – only through the disc circumference, simulating surface of the object, and excluding diffusion through open crack walls – was considered for the sake of clarity.

Free triangular mesh patterns were used to discretize object geometry in solid mechanics module of COMSOL including geometry nonlinearity for the study. Mesh was optimized to ensure proper spatial and temporal evolution of moisture profile in wood. The size distribution of mesh elements was determined using a criterion that ΔRH between neighbouring mesh elements could not reach 1% for an RH step change from 50% to 20%. The smallest mesh elements of size 40 µm were located close to the circumference and their size was growing in the direction towards disc's centre where their size was 1mm, which value was set as a maximum limit. Only one-eighth of the disc, containing the crack, was meshed with such strict conditions. In the remaining part, the mesh element size was multiplied by 20 but kept not larger than 10 mm to reduce computation time of the simulations. The number of domain elements was approximately 60 thousands.

Similar approach was applied to optimize time steps Δt during calculation of impact of an instantaneous RH change. As a criterion of optimisation, maximal value of 1% ΔRH was accepted between time instant t and $t+\Delta t$ for the same step change. It was found that Δt grew exponentially in course of time starting from 0.4 s to 630 hours, during simulation of 6 months. For simulations of sinusoidal RH changes, Δt constituting ca. 0.01 of sine period T_{sin} was used. For such a step, the accuracy of the sinusoidal model was sufficient.

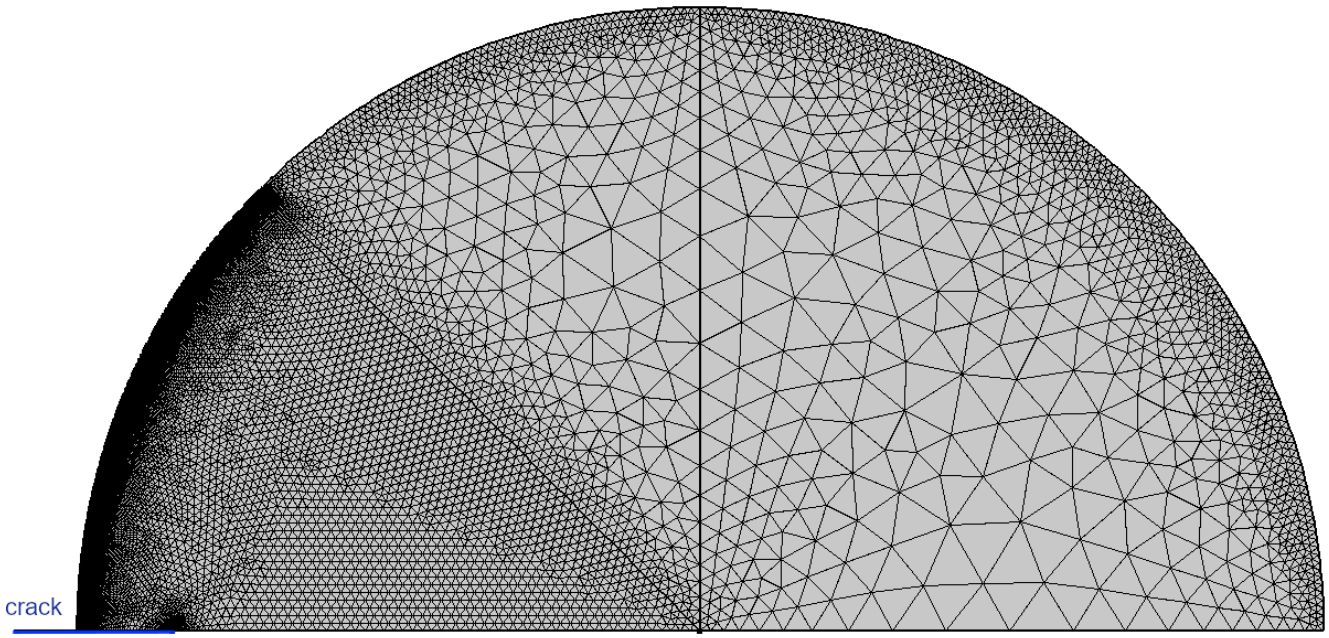

Fig.2 Model of a massive wooden sculpture reduced to simple geometry. Small area with finer mesh elements surrounds tip of the 10 mm deep crack that is depicted with a blue horizontal line

It is assumed that the object modelled is made of pine wood (*Pinus sylvestris),* the species relevant for the Norwegian wooden churches being in focus of the research projects indicated in the Acknowledgments. Material parameters required as the model input are given in detail below. Mechanical properties of wood strongly depend on MC, therefore, where possible, all parameters were expressed as a function of MC.

Water vapour adsorption and desorption isotherms of pine wood measured by Bratasz et al. (2012) were used to calculate scanning isotherm – an intermediate curve between the adsorption and desorption branches - according to the procedure developed by Mualem (1974) to account for the effect of sorption hysteresis in wood. The scanning

isotherm is compared with sorption of pine wood given by other authors (Fig.3). The polynomial function was fitted to the experimental data and was used in the model (Eq.3):

$$MC = 1.123 + 0.448 \cdot RH - 0.012 \cdot RH^2 + 2.204 \cdot 10^{-4} \cdot RH^3 - 2.080 \cdot 10^{-6} \cdot RH^4 + 8.833 \cdot 10^{-9} \cdot RH^5 \quad (3)$$

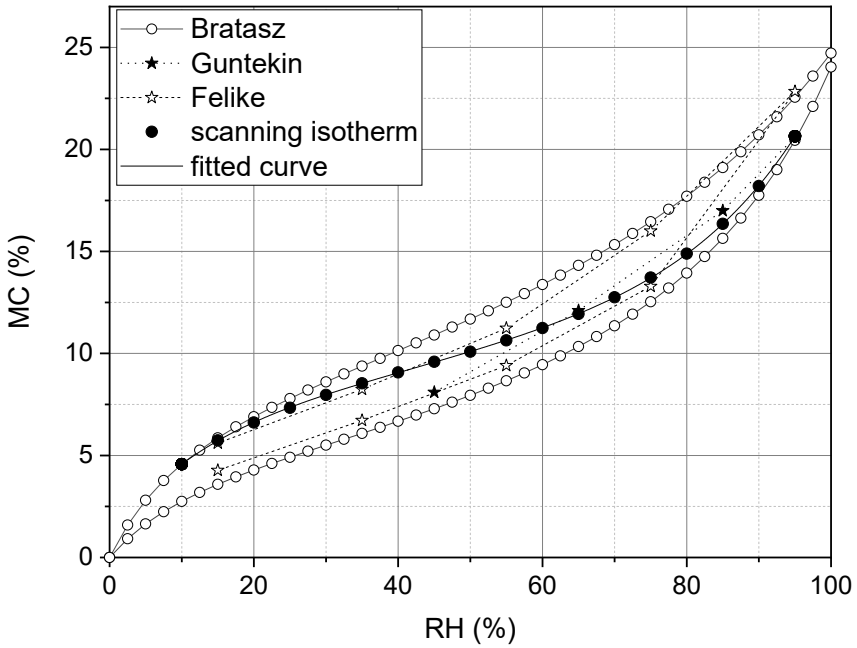

Fig. 3 Comparison of scanning water vapour sorption isotherm for pine wood calculated from Bratasz et al. (2012) with the experimental data of Güntekin and Akar (2019) and Felike et al. (2011)

Mechanical parameters of pine wood used in the model were taken from Güntekin and Akar (2019) who determined them experimentally as a function of MC. Young moduli in the R and T directions are compared with values given by other authors (Aira et al. 2014; Dinwoodie 2004; Danielsson and Gustafsson 2013; Pencik 2013; Kossakowski 2009) in Fig. 4 a and b.

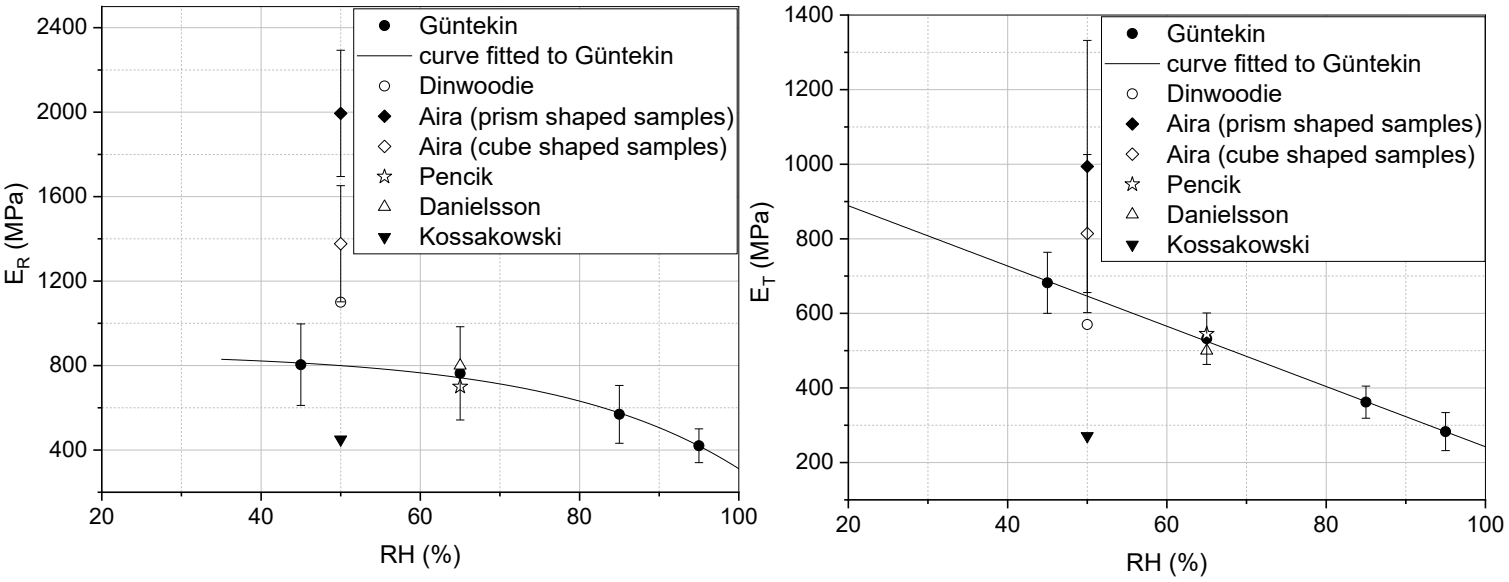

Fig.4 Young modulus of pine wood as a function of RH in the radial (**a**) and tangential (**b**) directions (references to the publications are provided in the text)

Shear modulus in the RT-direction was also deduced from values measured by Güntekin and Akar (2019) by fitting exponential function: $G_{RT} = -0.07 \exp\left(\frac{RH}{14.97}\right) + 109.49$ where G_{RT} is in MPa and RH is in %. The dispersion of Poisson's ratio values for different MC given by Güntekin and Akar (2019) was insignificant, therefore, the average value for the TR-direction was calculated and used, $\nu_{TR} = 0.59$. Other Poisson's ratio values are related to ν_{TR} due to the symmetry of strain and stress tensors and calculated within the COMSOL software according to Eq. 4 resulting from the symmetry of the compliance matrix:

$$\nu_{xy} = \nu_{yx} \frac{E_x}{E_y} \tag{4}$$

Hygric dimensional change of pine was adopted after experimental work performed by Bratasz et al. (2010). However, instead of a linear dependence applicable for an MC range of 5-15%, the sigmoid dependence (Eq.5) describing the whole MC range was adopted and its parameters are given in Table 1:

$$\alpha(MC) = \alpha_{max} \frac{MC^n}{k^n + MC^n} \tag{5}$$

Table1 Parameters of the sigmoid function (Eq.5) describing hygric dimensional change of pine wood

Anatomical direction of wood	α_{max}	k	n
Radial	4.96	32.93	1.27
Tangential	12.46	34.84	1.30

It was assumed for simulations of a step RH change that, at 50% RH, the object is in a stress free state. The selection is justified as 50% is the universally accepted optimal long-term RH level for mixed collections in museums. For sinusoidal variations, the stress free state was assumed at the RH level corresponding to the average MC in wood. The RH level thus defined is different from 50% - the level at which sinusoidal variations are centered – due to an increase of the water vapour diffusion coefficient with RH and the upswing of the water vapour sorption isotherm at the high RH range. Density of pine wood was adopted from the work of Repola (2006) who tested pine samples from 38 Scots pine stands in Finland, ρ = 413 kg/m^3. That value is lower than one reported by Güntekin and Akar (2019) but is in the range of values ven by Bertolin (2021) in her review.

Model parameters describing diffusion were assumed to follow a relationship between water vapour diffusivity D in wood and RH proposed by Time (1998) with a temperature modification factor proposed by Simpson (1993):

$$D(RH, T) = 1.44 \cdot 10^{-7} RH^{1.8449} \exp\left(\frac{-5280}{T}\right) \tag{6}$$

where D is in kg/msPa and T is temperature in K. The barrier of an air forming a layer adjacent to the object's surface slows down water vapour transport through the wood surface. To account for this resistance, external mass transfer coefficient h' in kg/m^{2}sPa was used after Time (1998), $h' = 3 \cdot 10^{-8}$. Value of the parameter depends on the intensity of air movement in a specific environment and, in this study, it reflected environments with a considerable air motion typical of museum galleries and interiors of historic buildings.

Mathematical modelling

Partial differential equation of diffusion solved during simulation, describing the movement of water vapour in the disc as well as into or out of the wood, was:

$$\rho C_M \frac{\partial \varphi}{\partial t} + \nabla \cdot \boldsymbol{J} = 0 \tag{7}$$

$$\boldsymbol{J} = -D\nabla p \tag{8}$$

with boundary conditions:

$$RH = RH_0 \tag{9}$$

$$-\boldsymbol{n} \cdot \boldsymbol{J} = h' \cdot p_{sat}(T) \cdot \Delta\varphi \tag{10}$$

where ρ is the density in kg/m^3, $C_M = \frac{\partial MC}{\partial RH}$ is the specific moisture capacity at constant temperature, RH is relative humidity, φ is the water activity equal to $RH/100$. $\boldsymbol{J}$ is the moisture flux in kg/m^{2}s, D is the diffusion coefficient in kg/msPa, p, p_{sat} stand for pressure and saturation pressure of water vapour, respectively, in Pa, and h' is external mass transfer coefficient in kg/m^{2}sPa.

Gradient of moisture distribution in wood generates a stress field owing to the internal restraint to the free dimensional change across the wood. Stress tensor $\boldsymbol{\sigma}$ and resulting elastic strain tensor $\boldsymbol{\varepsilon}$ are related through the Hooke's law:

$$\boldsymbol{\varepsilon} = \boldsymbol{S}\boldsymbol{\sigma} \tag{11}$$

where $\boldsymbol{S}$ denotes the compliance matrix. For the orthotropic material in two-dimensional space compliance matrix size is reduced to 4 independent constants:

$$\boldsymbol{S} = \begin{bmatrix} \frac{1}{E_R} & -\frac{\nu_{RT}}{E_R} & 0 \\ -\frac{\nu_{RT}}{E_R} & \frac{1}{E_T} & 0 \\ 0 & 0 & \frac{1}{G_{RT}} \end{bmatrix} \tag{12}$$

In Eq.12, E is the elasticity modulus in Pa, ν is the Poisson's ratio, and G_{RT} is the shear modulus in Pa related to the respective wood directions R and T. Constants of the compliance matrix are calculated using mechanical parameters of pine wood from the above paragraph.

Fracture mechanics

J-integral developed by Rice (1968) is a method widely used in computational fracture mechanics analyses. In the elastic materials, *J*-integral is equal to *G* associated with crack propagation in x_1-direction, therefore $G = J_1$. However, this classical approach cannot be applied for nonhomogeneous bodies as it loses its main feature - path independence. The alternative version was proposed instead, in which the integral rather than being calculated over the line contour was reformulated to the form that could be integrated over the closed area surrounding the crack tip – the equivalent domain integral.

Due to the analogy of heat and moisture diffusion described in the previous paragraph, equations 13-17 formulated by Hein and Kuna (2017) for two-dimensional crack problem in Functionally Graded Materials subjected to thermal shock are suitable for studying fracture processes in wood experiencing RH variations:

$$G = J_1 = \lim_{r\to 0} \int_{C_C} \left(U\left(x_i, \boldsymbol{\varepsilon_{ij}^m}, RH\right)\boldsymbol{n_1} - \boldsymbol{t_i u_{i,1}}\right) \mathrm{d}s = \lim_{r\to 0}(-\widetilde{I_1} - \widetilde{I_2} + \widetilde{I_3}) \tag{13}$$

with

$$\widetilde{I_1} = \int_{A_C}\left(\frac{1}{2}\boldsymbol{\varepsilon_{ij}^m}\frac{\partial \boldsymbol{C_{ijkl}}}{\partial x_1}\boldsymbol{\varepsilon_{kl}^m} + \frac{1}{2}\boldsymbol{\varepsilon_{ij}^m}\frac{\partial \boldsymbol{C_{ijkl}}}{\partial RH}\boldsymbol{\varepsilon_{kl}^m}\frac{\partial RH}{\partial x_1} - \boldsymbol{\sigma_{ij}}\left(\left(\frac{\partial \boldsymbol{\alpha_{ij}^{RH}}}{\partial x_1} + \frac{\partial \boldsymbol{\alpha_{ij}^{RH}}}{\partial RH}\frac{\partial RH}{\partial x_1}\right)\Delta RH(x_i) + \boldsymbol{\alpha_{ij}^{RH}}\frac{\partial \Delta RH(x_i)}{\partial x_1}\right)\right)q\,\mathrm{d}A \tag{14}$$

$$\widetilde{I_2} = \int_{A_C}(U\boldsymbol{\delta_{1k}} - \boldsymbol{\sigma_{ik}}\boldsymbol{u_{i,1}})q_{,k}\,\mathrm{d}A \tag{15}$$

$$\widetilde{I_3} = \int_{C^+ + C^-}(U\boldsymbol{n_1} - \boldsymbol{t_i}\boldsymbol{u_{i,1}})q\,\mathrm{d}s \tag{16}$$

Hereby, $U\left(x_i, \boldsymbol{\varepsilon_{ij}^m}, RH\right)$ is the elastic strain energy density being a function of the elastic strain $\boldsymbol{\varepsilon_{ij}^m}$, the relative humidity RH and coordinate x_i. $\boldsymbol{t_i} = \boldsymbol{\sigma_{ij}}\boldsymbol{n_j}$ denotes the traction vector on the contour derived from the stress tensor $\boldsymbol{\sigma_{ij}}$ and the outward normal vector $\boldsymbol{n_j}$. $\boldsymbol{u_{i,1}}$ is the displacement vector.
It must be noted that a comma after an item $(\cdot)_{,i} = \partial(\cdot)/\partial x_i$ means partial differentiation with respect to coordinate x_i.
$\boldsymbol{C_{ijkl}} = \boldsymbol{S_{ijkl}}^{-1}$ is the elasticity tensor, related to the compliance tensor $\boldsymbol{S_{ijkl}}$. $\boldsymbol{\alpha_{ij}^{RH}}$ is hygric expansion tensor. $\boldsymbol{\delta_{mj}}$ stands for Kronecker's unity tensor.
A_C represents a domain surrounded by the closed contour $\tilde{C} = C + C^+ - C_C + C^-$ as shown in Fig. 5 and ds and dA are infinitely small elements of contour and area, respectively.

$q = q(x_i)$ is a function varying smoothly within areal domain A_C:

$$q(x_i) = \begin{cases} 0 \text{ on } C \\ 1 \text{ on } C_C \end{cases} \tag{17}$$

In this study, mode I loading is investigated, which causes the third term of *J*-integral, $\widetilde{I_3}$, to disappear due to the fact that $\boldsymbol{n_1}$ and traction components $\boldsymbol{\sigma_{22}}$ and $\boldsymbol{\sigma_{12}}$ are zero on the crack surfaces C^+ and C^- as explained by Yildirim (2006).

Internal radius of the integration area A_C in the model was chosen after optimization as described in the following paragraph.

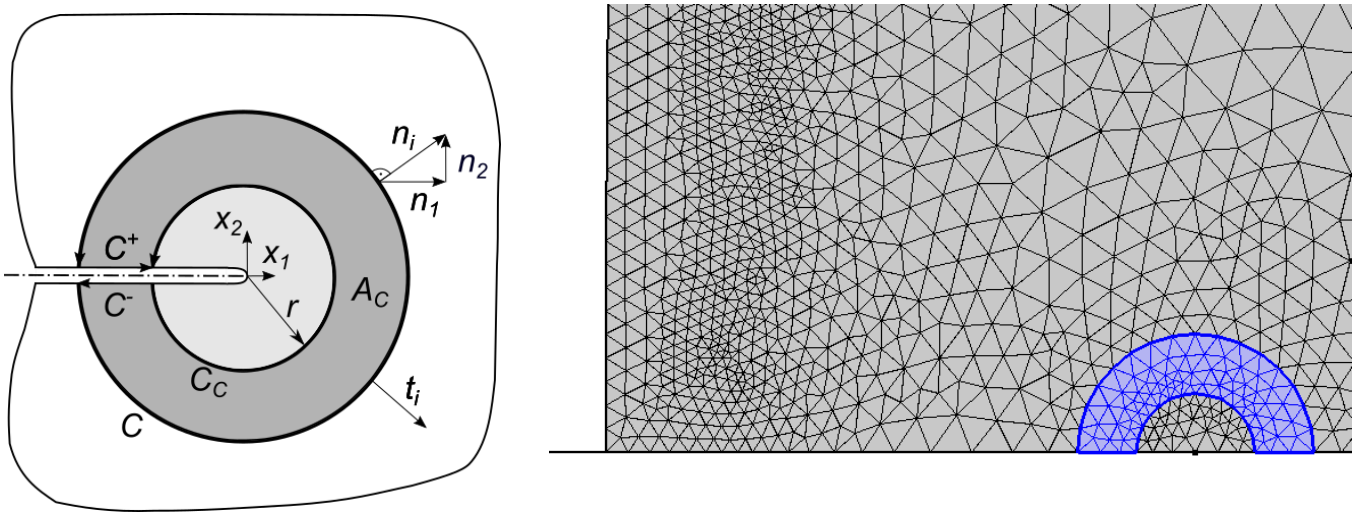

(a) (b)

Fig.5 a Integration paths around the crack tip after Hein and Kuna (2017), **b** integration paths in the finite element analysis, a highlighted domain is an integration area and a thicker line represents wall of the 220 µm deep crack

Optimization of the integration area size

Path-independence is the main feature of J-integral, which in case of the domain form of integral means that area of integration can be chosen arbitrarily. However, since the finite element model uses numerical approximations, the integration area needs to be chosen carefully to ensure convergence of the solution. In this study, the integration area was chosen as area between two circles of internal and external radii r and 2r, respectively whose centres were at the crack tip. The numerical optimisation was performed for a crack of 10 mm depth, a constant temperature of 21°C and an RH change between 50 and 20%. The maximum of *G* was reached after 900 hours. Several lengths of the inner radius were studied. It was observed that a too small radius led to overestimation of the G value which stabilized for the inner radii larger than 100 µm. The results are depicted in Fig. 6. On the other hand, integration area size cannot be larger than size of the crack. The inner radius optimal value of 100 µm was selected for further calculations.

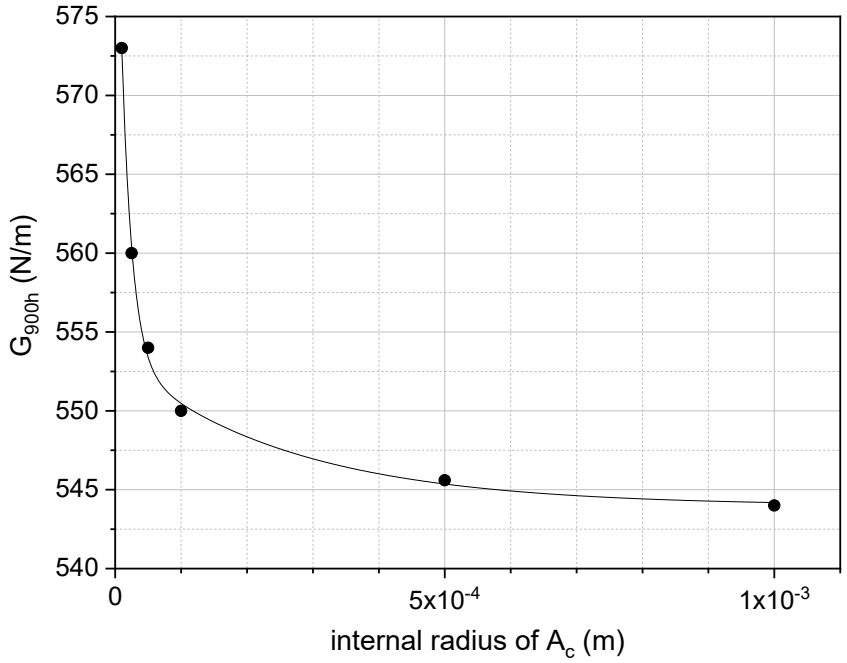

Fig.6 *G* for a 10 mm deep crack after 900 hours as a function of the internal radius of the A_C

Fracture criterion

Crack propagates in material when *G* reaches critical level G_{Ic}. G_{Ic} is a material-specific value and, for wood, it depends on the geometry as well as on MC which is related with RH through the scanning isotherm (see Fig. 3). G_{Ic} for pine wood at different humidity levels was determined by Vasic and Stanzl-Tschegg (2007) in the mixed experimental-numerical study. Values for the TR-direction are presented in Fig.7. A Lorentzian peak function with the baseline fixed at 250 N/m was fitted to the data points in order to approximate G_{Ic}-RH dependence in the whole RH range.

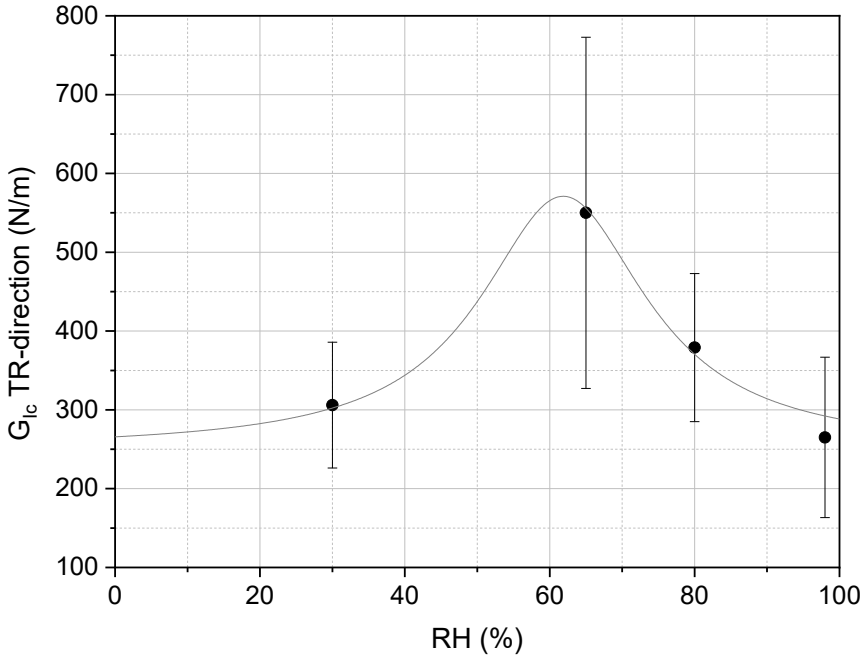

Fig.7 G_{Ic} for pine as a function of RH measured by Vasic and Stanzl-Tschegg (2007), a grey line represents a Lorentzian peak function fitted to the data points

Results and discussion

G for a step change of RH

The smallest crack size used in the calculations was 70 μm. Flaws of such scale are believed to exist with high probability in each wood sample. The largest crack size of 60 mm used in the calculations was slightly smaller than the radius of the modelled disc. Crack depths studied were chosen to grow logarithmically with three values per each decade. Several additional values were also taken into account when it was needed.

Results of the simulation for an instantaneous drop ΔRH of 30% from the initial RH level are presented in Fig. 8. Data for cracks shallower than 220 µm is not plotted due to the marginal values of G obtained. After the RH drop, the new humidity was maintained for infinite time but only first 6 months after the beginning of drying are plotted in Fig.8. Solid lines represent G as a function of time, whereas dashed lines stand for G_{Ic} plotted for each crack depth individually. Dashed lines were deduced from the value of RH at the crack tip correlated to the corresponding G_{Ic} as in Fig.7. Colours of the lines match the specific crack depth.

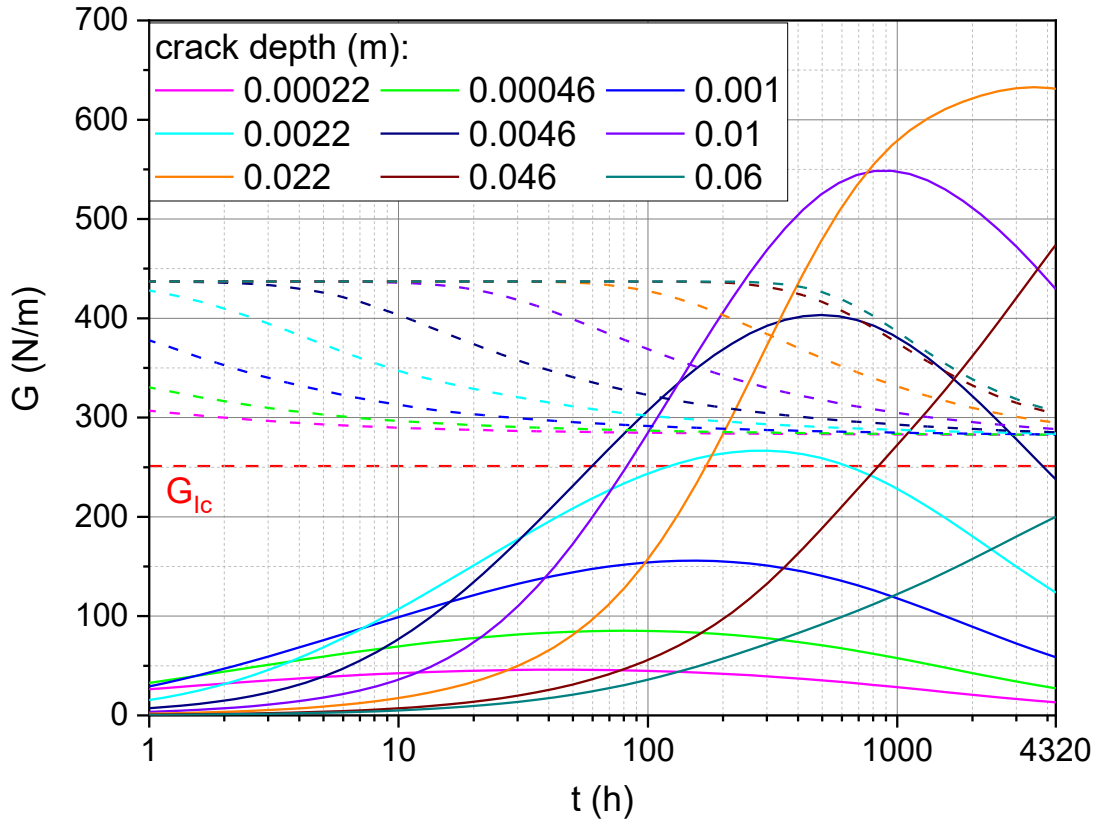

Fig.8 G (solid lines) and its critical value (dashed lines) as a function of time for an RH change 50 → 20%. A horizontal red dashed line illustrates G_{Ic} of a constant value independent of MC of wood

G_{Ic} decreases as drying front propagates towards the disc centre. On the other hand, the same process causes an increase of G value until the drying front reaches the crack tip, and then slowly decreases. It can be observed that the deeper the crack, the longer it takes for the drying front to reach the crack tip. Intersection of solid and dashed lines for a specific crack depth indicates the beginning of fracture propagation. However, in order to consider the worst case scenario and, therefore, eliminate false negative predictions, it was assumed that critical value of G_{Ic} was 250 N/m corresponding to the G_{Ic} baseline in Fig.7. That critical value is depicted in Fig. 8 by a horizontal red dashed line.

It can be observed that G for cracks shallower than 2.2 mm do not reach a critical value, independently of duration of the RH change to which the wooden disc representing a sculpture is exposed, thus they are stable. For the crack depths between 2.2 mm and 46 mm, further fracture will occur if the dry conditions are maintained over time sufficient for the drying front to reach the crack tip. The shortest time of ca. 60 hours necessary for a crack to propagate was found for depth of 4.6 mm. If the crack's initial depth is 60 mm, 6 months are not enough for the crack extension owing to slow diffusion of moisture into the core of a massive object, where the crack tip is located.

The obtained results were also plotted in the form of the two-parameter risk map in Fig. 9.

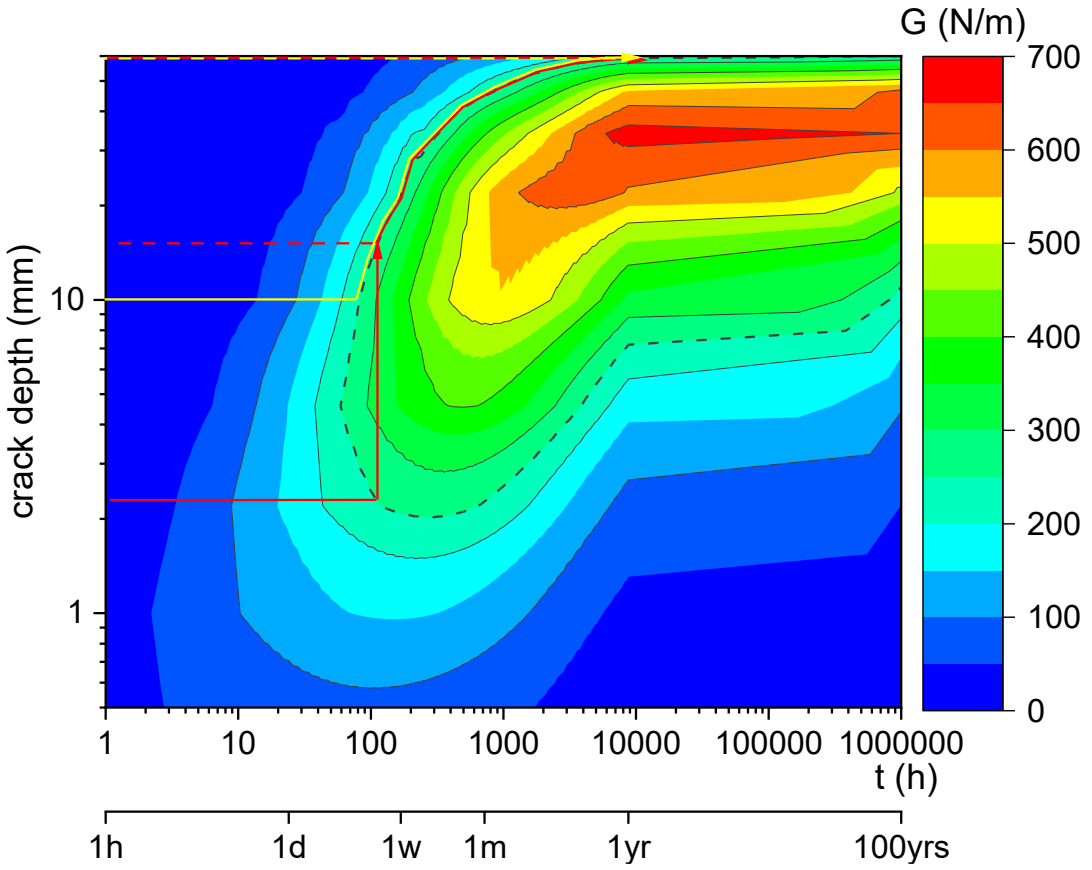

Fig.9 Two-parameter risk map for an RH change 50 → 20% showing crack depth (*y* axis) as a function of time of drying (*x* axis) and corresponding *G* (isolines). G_{Ic} is represented by a black dashed line. Two scenarios are possible for a flaw propagation in material depending on the initial crack depth: catastrophic growth (red lines), continuous propagation process (yellow lines). Coloured dashed lines mark the depth of the extended crack

The map depicted in Fig. 9 helps to analyse and interpret the crack propagation by selecting crack depth and duration of an RH variation. For the given crack depth and duration, one can estimate the length of the crack's extension. As shown in Fig. 9, *G* increases with time for the given crack depth. When a chosen combination of crack depth and duration results in reaching the critical value of 250 N/m, a flaw in material starts to propagate.

Two scenarios are possible for crack propagation (Fig. 9). Catastrophic crack growth occurs when the criterion of the critical energy is satisfied for a range of crack depths at one time instant. In Fig.9, after 100 h, *G* for all crack depths between 2.2 and 10.7 mm is greater than G_{Ic}. In consequence, crack of 2.2 mm depth instantaneously propagates to 10.7 mm and then continues to grow gradually as time progresses. Gradual crack growth occurs for cracks initially deeper than 10.7 mm along the 250 N/m isoline until the maximum depth of ca. 60 mm is reached. The growth is caused by the fact that, in the ultimate equilibrium state RH is 20% in the entire disc and *G* for 60 mm deep crack is still higher than G_{Ic}. Therefore, maintaining dry conditions for a long time will result in the development of a crack reaching the centre of the disc. As there is a singularity in the centre of the model, 60 mm depth is here considered as a full crack depth.

G value was also modelled for an RH drop from the initial 50% RH level to 30%. Results in the form of a map are presented in Fig. 10.

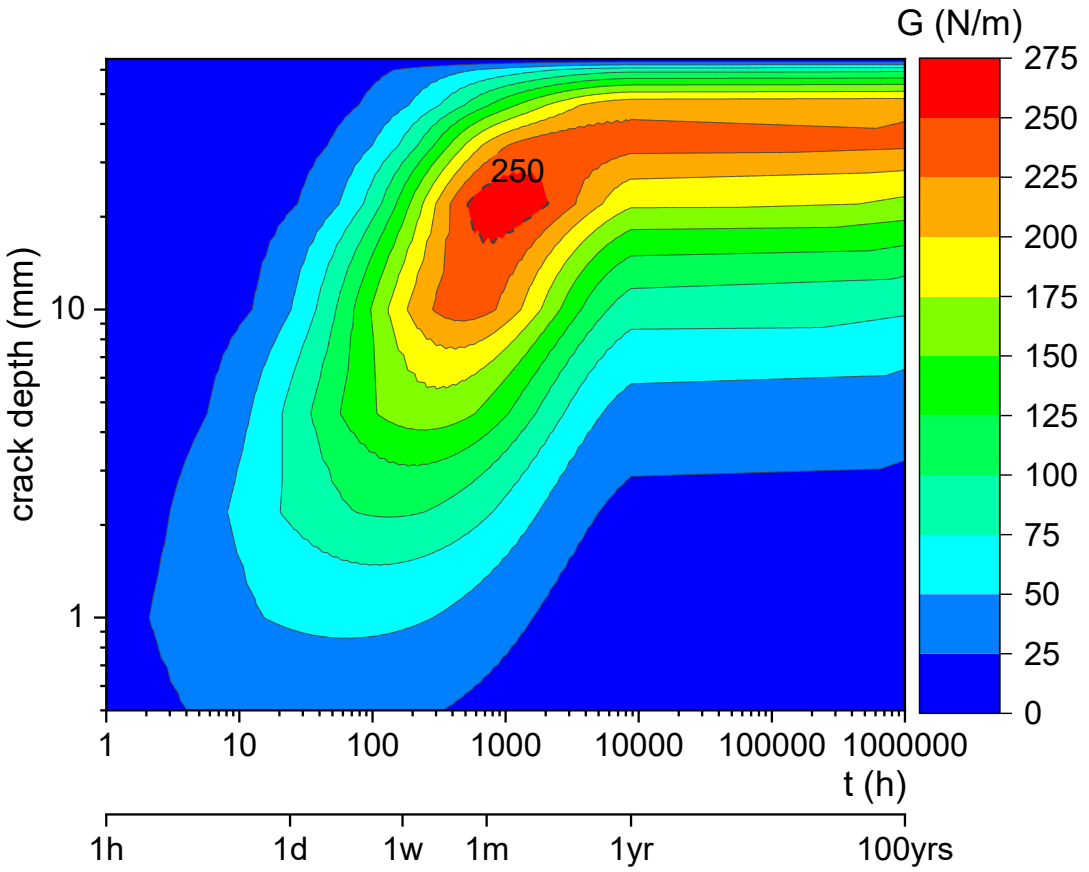

Fig.10 Two-parameter risk map for an RH change 50 → 30% showing crack depth (y axis) as a function of time of drying (x axis) and corresponding G (isolines). G_{Ic} is represented by a dashed line

The range of crack depths and times to fracture for which G values are greater than the critical level is reduced significantly.

Fig. 11 illustrates how G_{max}, which denotes the maximum value of G, is changing with varying ΔRH of step changes for various crack depths. As one can see, the dependence of G_{max} on the change magnitude increases nonlinearly. Interestingly, G_{max} increases with crack depth for cracks shallower than 2.2 mm and starts to decrease for deeper cracks with an exception of G_{max} value for 3.4 mm deep crack in which case ΔRH is higher than 26%. The minimal ΔRH that can generate crack propagation is 19%.

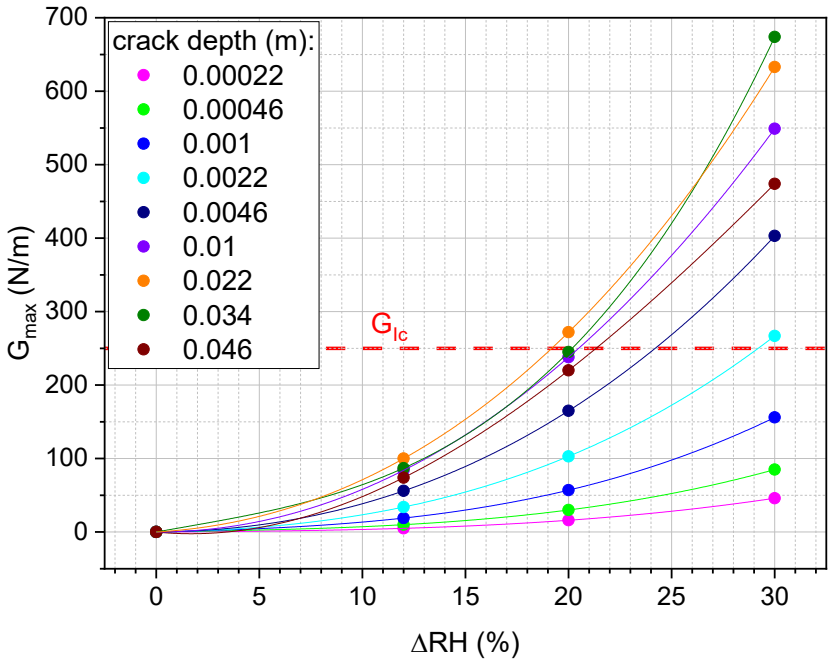

Fig.11 Maximum value of *G* as a function of magnitude of the RH drop

G for a sinusoidal change of RH

The step changes analysed earlier are relevant for the analysis of risks from very fast climatic events typical of large meetings of any kind or concerts but such changes do not reflect well risks from natural climate variability such as daily variations, weather or seasonal changes. Particularly, the seasonal variations are frequently the most pronounced RH cycles in heated buildings. Therefore, idealised microclimate variations in the form of sine function were analysed as well. Fig. 12 shows *G* as a function of time for the RH change in a form of sine function with period of 7 days and amplitude of 30% centred at the 50% level. During first 42 hours, the outer part of wood swells due to increasing RH inducing mainly compressive stresses in the radial direction. Insignificant tensile stresses are generated around the crack tip, which is related to the effect of the Poisson's ratio on the system. *G* starts to rise when RH drops below 50% and reaches peak value when RH is 20% with an increasing delay for deeper cracks.

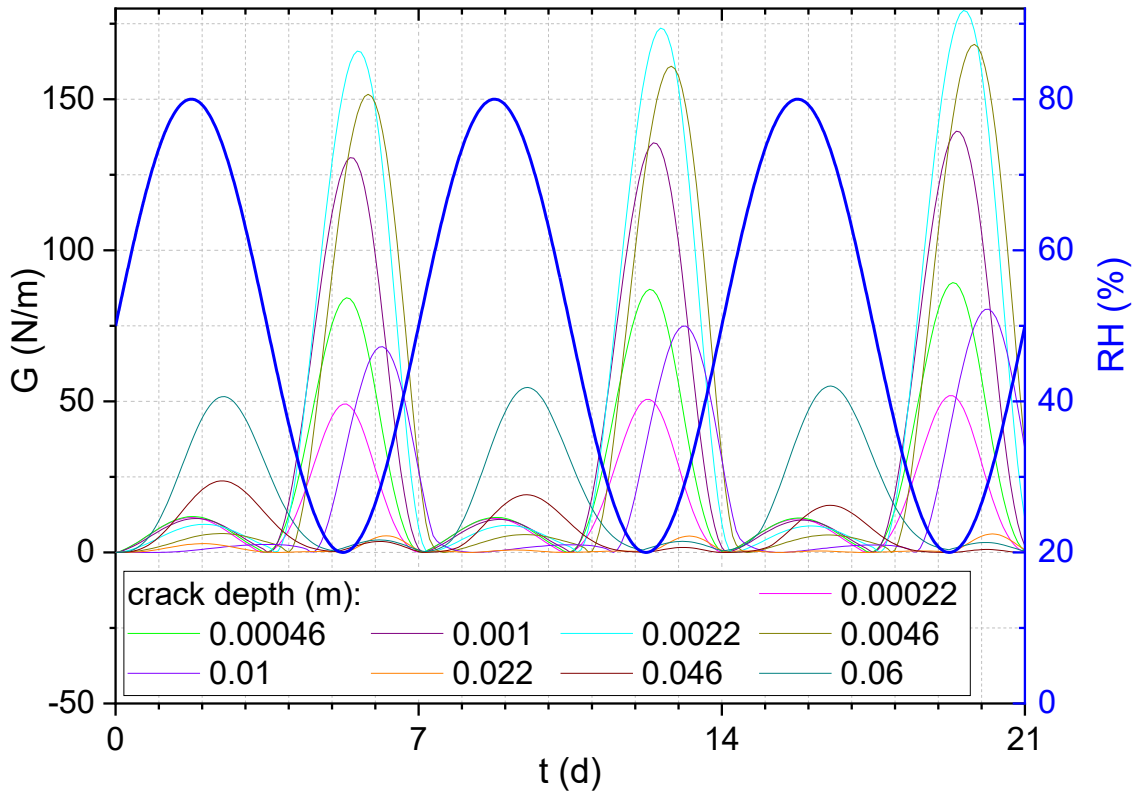

Fig.12 *G* as a function of time for a sinusoidal RH variation with period of 7 days and amplitude of 30% centred at the 50% level

Fig.12 shows that *G* value at the peak increases with each full period of the sine RH variation. This reflects evolution of moisture profile during repeated RH cycles caused by diffusion coefficient increasing with RH (see Eq. 6) and the upswing of water vapour sorption in the high RH region (see Fig. 3), as explained below. In order to eliminate this effect, simulations were performed for each sine period T_{sin} until moisture distribution became fully periodic. For T_{sin} of 1day, periodicity in the moisture profile was reached after 103 cycles and for longer sine periods after less than 16 cycles. In order to standardize the method, the moisture profiles for the subsequent simulations were extracted after 60 cycles for all T_{sin} values except for T_{sin} of 1 day, in which case it was extracted after 120 repeated sine cycles. The same equilibrated moisture distribution for each T_{sin} at t = 0 was applied as an initial condition in the model for each crack depth. During repeated sinusoidal cycling, an increase in the water vapour diffusion coefficient with RH causes the increase of average MC above the reference level of 10.1% corresponding to 50% RH as more moisture is gained when RH is higher than 50% than is lost during the drop of RH below 50% in the second half of the sine cycle. Higher diffusion coefficient causes an increase of the moisture content in the entire object, while the upswing of water vapour sorption isotherm affects the area reached by the drying/wetting front. The effect of these phenomena can be seen in Fig.13 in the non-symmetric moisture distribution profiles inside the modelled disc obtained at 20 time instants within one full sine RH cycle, calculated after the same cycle had been repeated 60 times. An average MC distribution along the disc's radius is represented by a red line.

In further calculations, it was assumed that RH level at which the object is free of stress corresponds to the plateau of average MC reached in wood with increasing distance from the surface. Fig.14 shows how the RH level corresponding to the stress free state varies depending on T_{sin}. The level reaches maximum of 57% for sine variations of periods ranging from 7 to 90 days. That 7% shift of the RH level corresponding to the stress free state significantly increases

the risk of cracking of massive wooden objects that has never been observed before. When sine variation becomes very long, the impact of diffusion coefficient increase with RH is diminished and only the shape of water vapour sorption isotherm affects the RH level corresponding to the stress free state, which gradually reaches 52.9%.

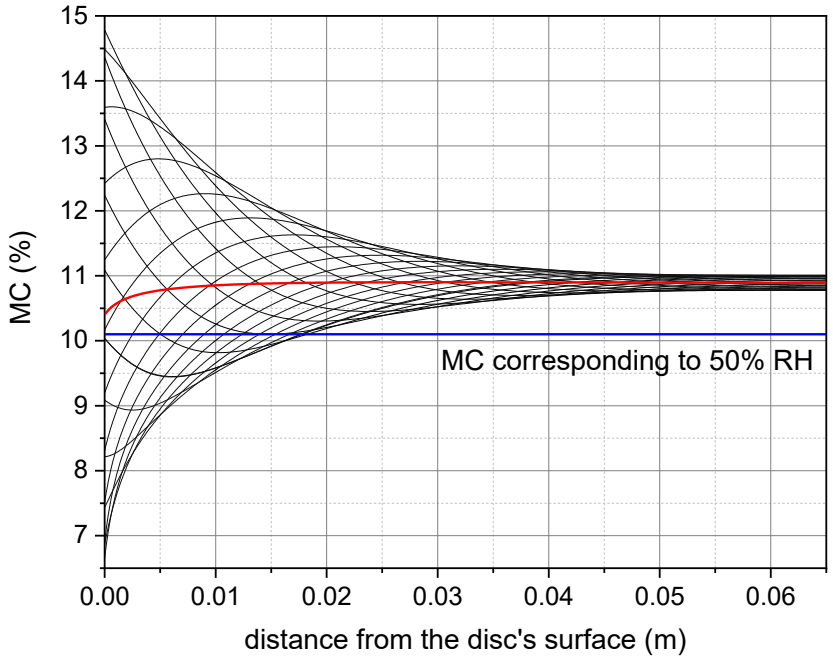

Fig.13 Moisture distribution profiles at 20 time instants within one sine RH cycle of T_{sin} of 30 days. A red line depicts an average MC from all the profiles. A blue line shows MC corresponding to 50%RH

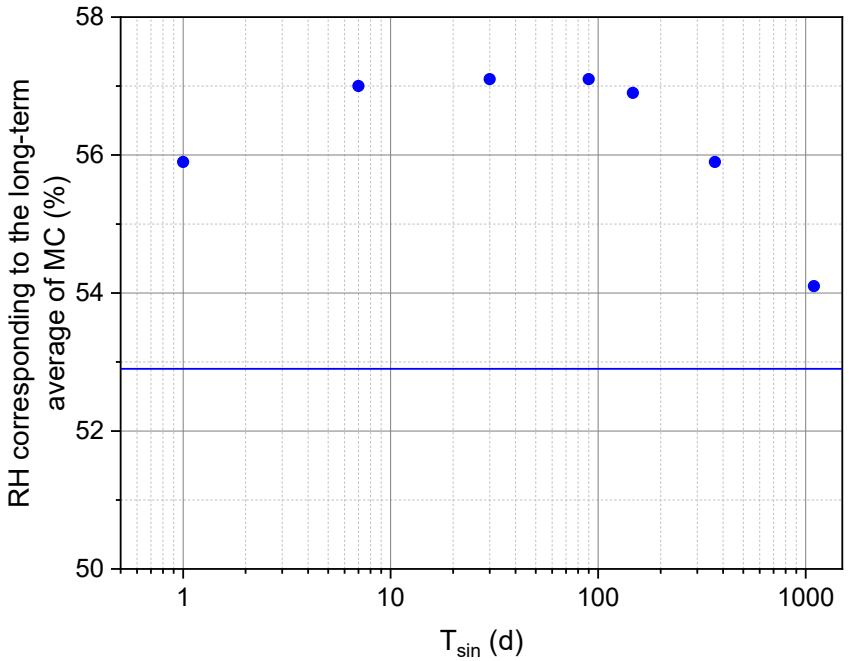

Fig.14 RH levels at which the object is assumed to be free of stress, depending on T_{sin}. For T_{sin} approaching infinity, this level tends towards 52.9% RH (a blue horizontal line)

Fig. 15 illustrates dependence of maximum value G_{max} for cracks of varying depth for a sine variation of amplitude of 30% centred at the 50% level and various periods T_{sin}. As one can see, this dependence has form of an asymmetric peak function, with the peak shifting toward longer T_{sin} for deeper cracks. The maximum G_{max} value of 850 N/m is reached for ca. T_{sin} of 147 days (21 weeks) and crack depth of 14 mm. One can see that longer variations corresponding to 90 and 147 days have similar and significantly higher peak values than shorter variations. Fig. 15 also shows that variations of T_{sin} shorter than 7 days do not reach the critical value of 250 N/m. One can observe that G_{max} values obtained as a result of a step change with ΔRH of 30% from the 50% initial level are significantly lower (even by 32% for a 14 mm deep crack) than the values that can be reached with a sinusoidal RH change.

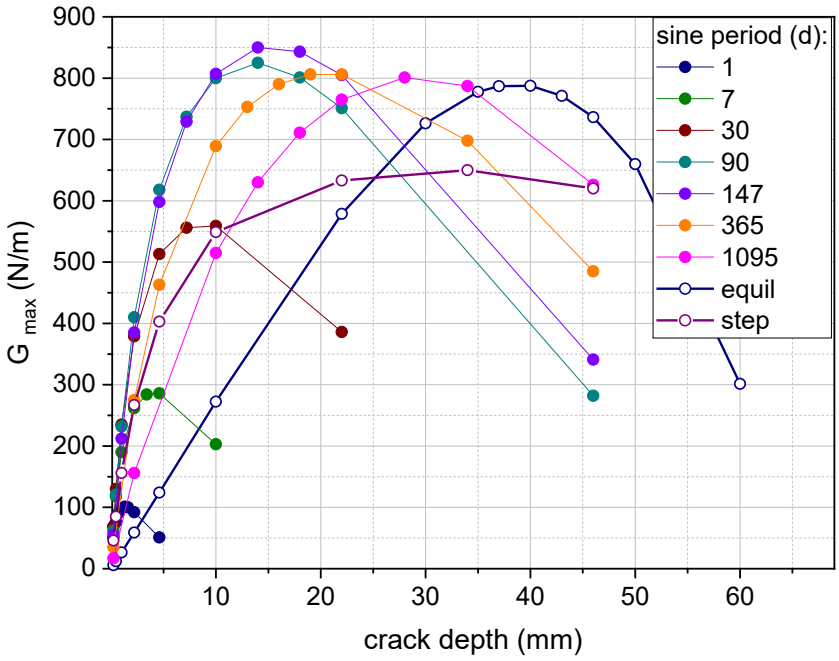

Fig.15 Maximum value of G reached during the full sine cycle as a function of crack depth. Empty circles denote results for two special cases: T_{sin} approaching equilibrium (equil) and a step change (step)

Fig.16 illustrates peak values of the G_{max} curves shown in Fig.15 and plotted as a function of T_{sin}. One can see that the critical value G_{Ic} is reached for T_{sin} of 5 days. The dependence is also characterized by a peak at T_{sin} = 147 and maximal value of $G_{max\ sin}$ = 850 N/m days after which $G_{max\ sin}$ values slightly decreases to the value of 788 N/m obtained for the equilibrium state.

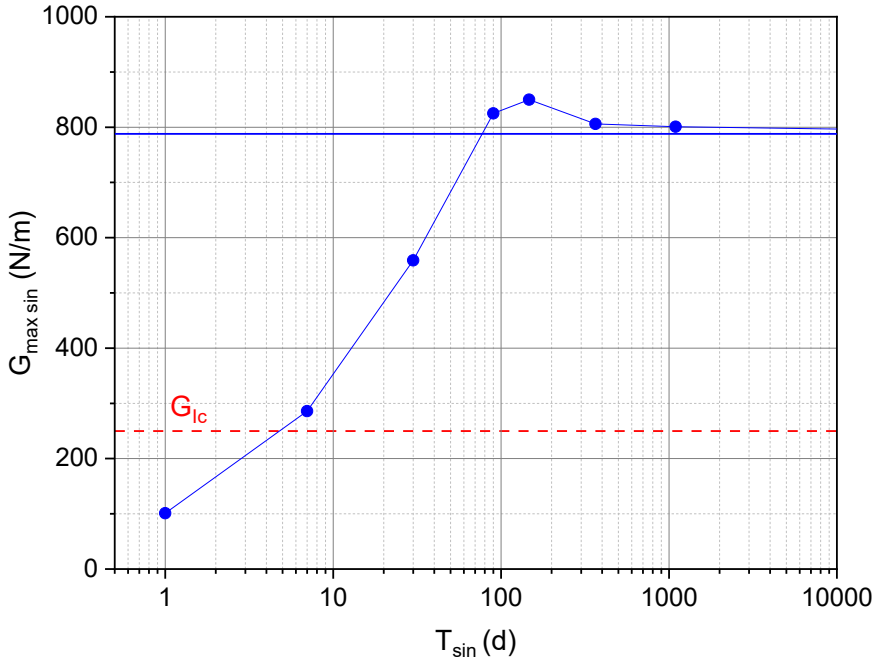

Fig. 16 $G_{max\ sin}$ corresponding to peak values of the G_{max} curves as a function of T_{sin}. Horizontal lines represent: red dashed - G_{Ic}, blue - solution for the T_{sin} approaching the infinity (equilibrium state)

Based on the dependence described and on the highest values of G obtained for T_{sin} of 147 days, critical ΔRH bringing G to G_{Ic} was estimated to be 16%. The estimation was confirmed by simulations for RH sine with period of 147 days and amplitude of 16% centred at the 50% level. As it can be seen in Fig. 17, the peak in the plot of G versus time was indeed lower than G_{Ic}.

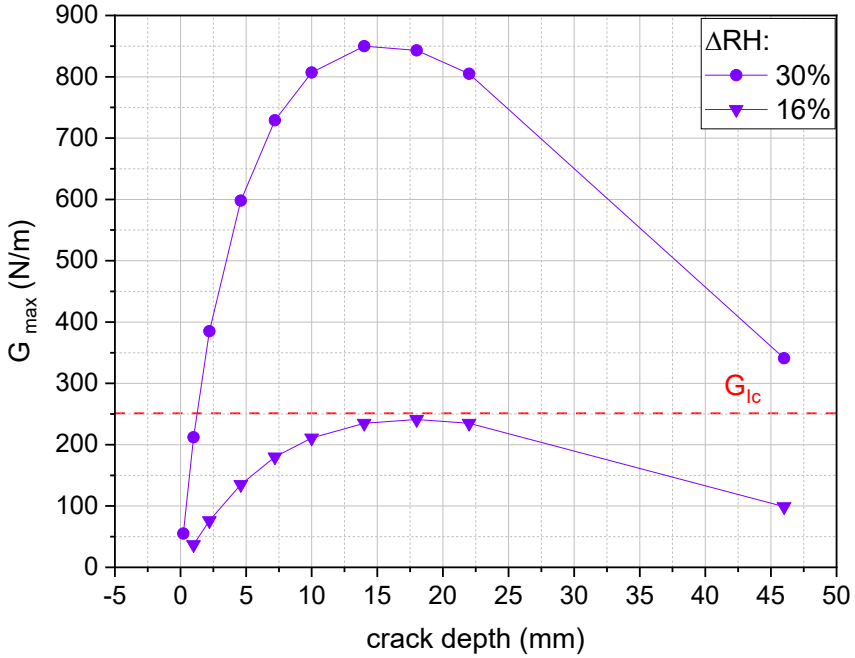

Fig. 17 Comparison of G_{max} obtained for T_{sin} of 147 days and two ΔRH: 16% and 30%. Moisture distribution profiles as well as free stress levels were adjusted to the RH change magnitude

Conclusion

A two-dimensional model of massive wooden cultural heritage objects was developed to analyse fracture processes induced by dynamic RH variations, generating gradients of MC across the wood. It was shown that a fracture mechanics method, developed for Functionally Graded Materials under thermal stress can be successfully used to study the impact of RH variations on cultural heritage objects like wooden sculptures or furniture.

The simulations performed for pine wood showed that the critical magnitude of a step RH drop from an initial 50% level is about 19%. *G* rose with increasing magnitude of the step change approximately as a cubic function. It was found that the RH variation needed to be prolonged enough to induce rise of *G* above the critical level and thus cracking in wood. It was also shown that cracks of depth larger than 2 mm were significantly more prone to propagation than shorter cracks. In fact, cracks shorter than 2 mm would not grow if ΔRH was smaller than 30%. The described observations have very important consequences for practical preventive conservation in museums and historic buildings as climatic variations even of magnitude of 30% will not cause any damage to wooden objects if only duration will be shorter than approximately 2 days. This opens a door to formulation of safe procedures for organising cultural, commercial and religious events in buildings housing vulnerable collections.

The paper shows that sinusoidal RH variations generate higher risk of wood cracking than a sudden drop in RH. The G_{max} values are about 30% higher in the case of an RH sine variation than a step change of the same amplitude. Therefore, sinusoidal variations represent the worst case in analysis of risk of fracture in massive wooden cultural heritage objects. It was shown that the largest amplitude of RH sine variation centred at 50% safe for such objects is 16%. Sine periods ranging between 90-150 days constitute the most endangering variations. Sine variations of amplitude 30% and centred at 50% do not induce a risk of fracture in wood if sine period is shorter than 5 days. The notable effect is that the average MC, and in consequence RH corresponding to the stress free state, shift toward higher levels due to increasing diffusion coefficient and the upswing of water vapour sorption with RH. The consequence of the above effect is that the acclimatization of an object to periodic RH variations leads to increased risk when the object is exposed to a sudden drop in RH. This situation might happen when an object is taken from a historic building with natural microclimate, for example a church, to a conservation studio of different average RH level. The safe, simple step, RH change, discussed in this paper in *G for a step change of RH,* needs to be reduced by 6% as shown in Fig.14. In cases of higher RH levels typical of historic buildings, this effect is expected to be more significant owing to larger increase of the diffusion coefficient and water vapour sorption with RH.

References

Aira JR, Arriaga F, Iñiguez-González G (2014) Determination of the elastic constants of Scots pine (Pinus sylvestris L.) wood by means of compression tests. Biosyst Eng 126:12-22

ASHRAE (2019) Museums, Galleries, Archives and Libraries. ASHRAE Handbook. Chap 24. American Society of Heating and Air-Conditioning Engineers, Atlanta

Bertolin C, Karvan P, De Rosa A, Javad Razavi SM, Berto F (2021) Relation between fracture characteristics and moisture content along longitudinal direction in a naturally drying Scots pine. Theor Appl Fract Mec 112. https://doi.org/10.1016/j.tafmec.2021.102911

Bratasz Ł, Kozłowski R, Kozłowska A, Rachwał B (2010) Sorption of moisture and dimensional change of wood species used in historic objects. In: Gril J (ed) Wood Science for Conservation of Cultural Heritage – Braga 2008: Proceedings of the International Conference held by COST Action IE0601. Firenze University Press, Florence, pp 11-16

Bratasz Ł, Kozłowska A, Kozłowski R (2012) Analysis of water adsorption by wood using the Guggenheim-Anderson-de Boer equation. Eur J Wood Prod 70:445-451

Dag S (2006) Thermal fracture analysis of orthotropic functionally graded materials using an equivalent domain integral approach. Eng Fract Mech 73:2802-2828

Danielsson H, Gustafsson PJ (2013) A three dimensional plasticity model for perpendicular to grain cohesive fracture in wood. Eng Fract Mech 98:137-152

Dinwoodie JM (2004) Timber. Its nature and behaviour. 2nd ed. E & FN Spon, London and New York

Felike T, Zimmer K, Fromm J, Larnøy E (2011) Sorption behaviour of Scots pine in Northern Europe. Proceedings of the 7th meeting of the Nordic-Baltic Network in Wood Material Science & Engineering. https://nibio.brage.unit.no/nibio-xmlui/handle/11250/2673119?show=full. Accessed 7 June 2021

Forsman K, Fredriksson M, Serrano E, Danielsson H (2021) Moisture-dependency of the fracture energy f wood: a comparison of unmodified and acetylated Scots pine and birch. Holzforschung. https://doi.org/10.1515/hf-2020-0174

Griffith AA (1921) The phenomena of rupture and flow in solids. Philos T Roy Soc A 221:582-293

Güntekin E, Akar S (2019) Influence of moisture content on elastic constants of Scots Pine wood subjected to compression. Drewno 62(204):41-53

Hamdi SE, Moutou Pitti R, Dubois F (2017) Temperature variation effect on crack growth in orthotropic medium: Finite element formulaion for the viscoelastic behavior in thermal cracked wood-based materials. Int J Solids Struc 115-116:1-13

Hamdi SE, Moutou Pitti R (2018) Numerical investigation of climate change impacts on European wood species vulnerability. Procedia Structural Integrity 13:523-528

Hein J, Kuna M (2017) A generalized J-integral for thermal shock analyses of 3D surface cracks in spatially and temperature dependent materials. Theor Appl Fract Mec 92:318-330

Irwin G (1957) Analysis of stresses and strains near the end of a crack traversing a plate. J Appl Mech-T ASME 24:361-364

Jakieła S, Bratasz Ł, Kozłowski R (2008) Numerical modelling of moisture movement and related stress field in lime wood subjected to changing climate conditions. Wood Sci Technol 42:21-37

Kossakowski PG (2009) Mixed-mode I/II fracture toughness of pine wood. Arch Civ Eng 55(2):199-227

Luimes RA, Sukier ASJ, Verhoosel CV, Jorissen AJM, Schellen HL (2018a) Fracture behaviour of historic and new oak wood. Wood Sci Technol 52:1243-1269

Luimes RA, Suiker ASJ, Jorissen AJM, van Duin PHJC, Schellen HL (2018b) Hygro-mechanical response of oak wood cabinet door panels under relative humidity fluctuations. Herit Sci 6:72

Luimes RA, Suiker ASJ (2021) Numerical modelling of climate-induced fracture and deformation in wood: Application to historical museum objects. Int J Solids Struc 210-211:237-254

Mecklenburg MF, Tumosa CS (1991b) An introduction into the mechanical behavior of paintings subjected to changes in temperature and relative humidity. In: Mecklenburg MF (ed) Art in Transit: Studies in the Transport of Paintings. Washington: National Gallery, pp. 173-214

Mecklenburg MF, Tumosa CS, Erhardt D (1998) Structural response of painted wood surfaces to changes in ambient relative humidity. In: Dorge V, Howlett FC (eds) Painted wood: history and conservation. The Getty Conservation Institute, Los Angeles, pp 464–83

Mecklenburg MF (2007) Determining the acceptable ranges of relative humidity and temperatures in museums and galleries, Part 1, Structural response to relative humidity. https://repository.si.edu/handle/10088/7056. Accessed 7 June 2021

Mualem Y (1974) A conceptual model of hysteresis. Water Resour Res 10:514-520

Pencik J (2015) Modelling of experimental tests of wooden specimens from Scots Pine (Pinus sylvestris) with the help of anisotropic plasticity material model. Drvna Ind 66(1):27-33

Phan NA (2016) Simulation of time-dependent crack propagation in a quasi-brittle material under relative humidity variations based on cohesive zone approach: application to wood. Dissertation, Université de Bordeaux

Porter AW (1964) On the mechanics of fracture in wood. For Prod J 14(2):325-331

Rachwał B, Bratasz Ł, Krzemień L, Łukomski M, Kozłowski R (2012) Fatigue damage of the gesso layer in panel paintings subjected to changing climate conditions. Strain 48:474–81

Repola J (2006) Models for vertical wood density of Scots pine, Norway spruce and birch stems, and their application to determine average wood density. Silva Fenn 40(4):673-685

Rice JR (1968) A path independent integral and the approximate analysis of strain concentration by notches and cracks. J Appl Mech 35:379-386

Schniewind AP, Centeno JC (1973) Fracture toughness and duration of load factor I. Six principal systems of crack propagation and the duration factor for cracks propagating parallel to grain. Wood And Fiber 5:152-159

Simpson WT (1993) Determination and use of mosture diffusion coefficient to characterize drying of northern red oak (Quercus-rubra). Wood Sci Technol 27:409-420

Stanzl-Tschegg SE, Tan DM, Tschegg EK (1995) New splitting method for wood fracture characterization. Wood Sci Technol 29:31-50

Time B (1998) Hygroscopic moisture transport in wood. Dissertation, Norwegian University of Science and Technology

Triboulot P, Jodin P, Pluvinage G (1984) Validity of fracture mechanics concepts applied to wood by finite element calculation. Wood Sci Technol 18:51-58

Vasic S, Stanzl-Tschegg S (2007) Experimental and numerical investigation of wood fracture mechanisms at different humidity levels. Holzforschung 61:367-374

Yeh B, Schniewind AP (1992) Elasto-plastic fracture mechanics of wood using the J-integral method. Wood Fiber Sci 24(3):364-376

Yildirim B (2006) An Equivalent Domain Integral method for fracture analysis of Functionally Graded Materials under thermal stresses. J Therm Stresses 29. https://doi.org/10.1080/01495730500499175